Electronic Supplementary Material (ESI) for ChemComm.

Supporting Information

Supramolecular pathway selection of perylenediimides mediated by chemical fuels

Jorge Leira–Iglesias, [a] Alessandro Sorrenti, [a] Akihiro Sato, [a] Peter Dunne, [a] and Thomas M. Hermans*[a]

[a] Laboratoire des systèmes complexes hors équilibre, Institut de Science et d'Ingénierie Supramoléculaires UMR 7006, Université de Strasbourg & icFRC. 8 allée Gaspard Monge 67083 Strasbourg Cedex, France.

Section 1. Synthesis of PDI-1.

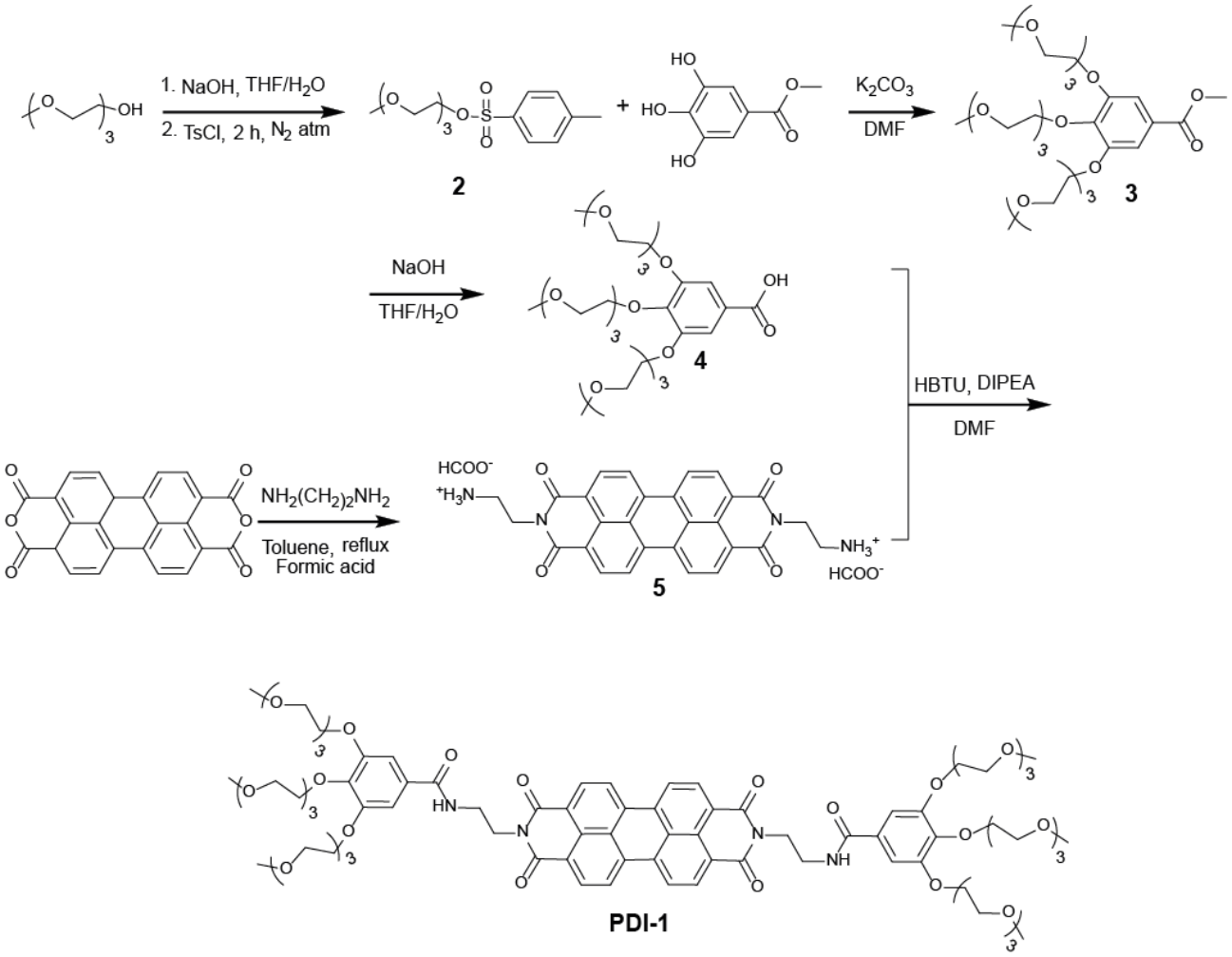

Scheme S1. Synthesis of **PDI-1**.

Methyl gallate was purchased from TCI chemicals. Triethyleneglycol monomethylether and perylene-3,4,9,10-tetracarboxylic dianhydride were purchased from Sigma-Aldrich. All other chemicals and solvents were purchased from Sigma-Aldrich and VWR. Purification of the reaction mixtures was performed by column flash chromatography using Geduran Si 60 silica gel (230-400 mesh). NMR spectra were recorded on a NMR Bruker AVANCE 400 MHz.

[2-[2-(2-Methoxyethoxy)ethoxy]ethoxy]p-toluenesulfonate (2). To a solution of triethyleneglycol monomethylether (10 g, 0.061 mol, 1 eq) in 20 mL THF, a solution of NaOH (5 g, 0.125 mol, 2 eq) in H_2O (20 mL) was added under stirring at 0 ºC. To this mixture, a solution of tosyl chloride (15 g, 0.078 mol, 1.3 eq) dissolved in 20 mL THF was added dropwise under inert atmosphere. Then, the reaction was allowed to warm to rt and stirred for 2 hours. Afterwards, 120 mL of diethyl ether were added and the organic layer was washed with 1 M NaOH (3 x 100 mL), water (2 x 100 mL), and dried over anhydrous $MgSO_4$. After evaporation and drying under vacuum, the tile product was obtained as a yellowish oil (18.53 g, 95%). ^{1}H NMR (400 MHz, $CDCl_3$) δ 7.84 (d, J = 8.3 Hz, 2H), 7.39 (d, J = 8.5 Hz, 2H), 4.25 –4.16 (m, 2H), 3.75 – 3.70 (m, 2H), 3.69 – 3.61 (m, 6H), 3.57 (dd, J = 5.8, 3.3 Hz, 2H), 3.41 (s, 3H), 2.49 (s, 3H).

Methyl 3,4,5-tris[2-[2-(2-Methoxyethoxy)ethoxy]ethoxy]benzoate (3). Methyl gallate (2 g, 10.8 mmol, 1 eq) and potassium carbonate (15 g, 108 mmol, 10 eq) were added to a solution of **2** (13.7 g, 43.2 mmol, 4 eq) in DMF (50 mL). The reaction mixture was heated at 80 ºC overnight under inert atmosphere. Then, the solvent was removed under vacuum and CH_2Cl_2 (100 mL) was added to the solid residue. The obtained solution was collected in a separatory funnel and washed with saturated $NaHCO_3$ (50 mL) and brine (50 mL). The organic layer was dried over anhydrous $MgSO_4$, followed by evaporation and drying under vacuum. Purification by flash chromatography using hexane/ethyl acetate (1:5) as eluent afforded **3** (6.02 g ,90%) as a yellow oil. ^{1}H NMR (400 MHz, $CDCl_3$) δ 7.31 (s, 2H), 4.23 – 4.19 (m, 6H), 3.88 (dd, J = 8.8, 3.6 Hz, 9H), 3.77 –3.70 (m, 6H), 3.70 – 3.62 (m, 12H), 3.56 (dd, J = 5.9, 3.2 Hz, 6H), 3.39 (s, 9H).

3,4,5-tris[2-[2-(2-Methoxyethoxy)ethoxy]ethoxy]benzoic acid (4). To a solution of **3** (6.02 g, 10.61 mmol, 1 eq) in 50 mL of a THF/H_2O 1.5:1 mixture at 0 °C, 10 mL of a 10.6 M solution of NaOH (100.61 mmol, 10 eq) were added. The reaction mixture was allowed to warm to rt and stirred overnight, after that, it was acidified to pH 2 with HCl (1 M) and extracted with CH_2Cl_2 (3 x 70 mL). The collected organic phase was dried over anhydrous $MgSO_4$, concentrated and dried under vacuum to give **4** (6.35 g, 98%) as a yellow oil. ^{1}H NMR (400 MHz, DMSO) δ 7.22 (s, 2H), 4.18 – 4.12 (m, 6H), 3.80 – 3.72 (m, 6H), 3.56 (m, 18H), 3.43 – 3.39 (m, 6H), 3.23 (s, 9H).

N,N'-bis(aminoethyl) perylene-3,4,9,10-tetracarboxylic diimide (5). To a suspension of perylene-3,4,9,10-tetracarboxylic acid dianhydride (0.25 g, 0.64 mmol, 1 eq) in 20 mL of toluene, 0.56 mL of ethylenediamine (8.9 mmol, 13 eq) were added in 10 min. The reaction mixture was refluxed overnight under inert atmosphere. After cooling down to rt, the obtained dark red precipitate was collected by filtration and then re-dispersed in 10 mL of aqueous KOH (5 M) and stirred overnight. Then, the red solid was filtered again, washed with H_2O, and dissolved in 10mL of formic acid. The insoluble fraction was filtered off, and 200 mL of isopropanol were added to the filtrate giving after precipitation, centrifugation and drying diimide **5** (0.12 g, 33%). ^{1}H NMR (400 MHz, D_2O) δ 7.98 (8H), 4.35 (4H), 3.33 (4H).

N,N'-Di[3,4,5-tris[2-[2-(2-Methoxyethoxy)ethoxy]ethoxy]benzoylaminoethyl]-perylene-3,4,9,10-tetracarboxylic diimide (PDI-1). Carboxylic acid **4** (0.157 g, 0.26 mmol, 2.4 eq) was dissolved in 20 mL of DMF. To this solution, HBTU (0.098 g, 0.26 mmol, 2.4 eq) and DIPEA (190 μL, 1.07 mmol, 10 eq) were added under inert atmosphere. After 5 min., diimide **5** (0.061 g, 0.11 mmol, 1 eq) was added and the reaction mixture was stirred at rt for 48 hours, after which 50 mL of CH_2Cl_2 were added. The organic phase was washed with saturated $NaHCO_3$ (2 x 50 mL) and brine, dried over anhydrous $MgSO_4$, and the solvent was evaporated under vacuum. Crude **PDI-1** was purified by flash chromatography using CH_2Cl_2/MeOH (gradient from 100:0 to 80:20) as eluent, followed by redissolution in CH_2Cl_2 (50 mL) and washes with 6 M HCl (3 x 50 mL) and brine, to remove traces of unwanted monosubstituted product. The organic phase was then dried over anhydrous $MgSO_4$ and concentrated to give pure **PDI-1** (0.112 g, 63%) as a red solid. ^{1}H NMR (400 MHz, DMSO) δ 8.70 (s, 4H), 8.48 (s, 2H), 8.39 (s, 4H), 7.00 (s, 4H), 4.55 (s, 12H), 4.28 (s, 4H), 4.03 (s, 16H), 3.78 – 3.40 (m, 68H), 3.19 (s, 18H). ^{13}C NMR (101 MHz, DMSO) δ 166.53, 163.38, 152.13, 140.20, 134.16, 130.05, 124.37, 123.12, 106.68, 72.30, 71.68, 70.29, 70.01, 69.31, 68.73, 63.49, 58.45. HRMS (ESI+) Calculated Mass for $C_{84}H_{112}N_4O_{30}Na_2$ [M+2Na$^+$]: 851.3573. Found: 851.3539.

Section 2. Methods

Electrochemical measurements. Electrochemical measurements were carried out with an Autolab type III μ-potentiostat using a 3-electrode setup consisting of a 2 mm glassy carbon working electrode, Pt foil counter electrode and either a Ag/AgCl reference electrode for aqueous baths or a Pt wire quasi-reference electrode for non-aqueous ones. Ferrocene was used as an internal reference and a method to determine the solution resistance in DCM (dichloromethane). Before each measurement, the working electrode was successively polished using 1 μm, 0.25 μm and 0.1 μm paste followed by ultrasonication in water, and for the non-aqeous bath a further sonication in DCM. The baths consisted of 0.1 M tetra-n-butylammonium hexafluorophosphate ($TBAPF_6$) and 0.1 mM **PDI-1** in DCM, and 2 mM gallic acid and 0.1 M KCl in water. All solutions were nitrogen purged for 1 hour prior to use, and all electrochemical measurements were carried out under a nitrogen blanket.

Sample preparation for 1 redox cycle. A solution was prepared by dissolving **PDI-1** (0.33 mg, 0.20 μmol) in 50 mM borate buffer, pH 8. Next, **PDI-1** was reduced (2 mL of 100 μM solution) adding 1 μL of a 400 mM $Na_2S_2O_4$ solution (in borate buffer) under stirring (note: the colour changes from cherry red to purple). The stirring in air caused the **PDI-1**$^{2-}$ to oxidize back to the neutral **PDI-1** in 2–3 minutes due to atmospheric oxygen (see Movie S1).

Sample preparation for multicycle experiments. Samples of **PDI-1** (2 mL, 100 μM) in 50 mM borate buffer were prepared analogously to the 1 cycle preparation (see paragraph above). Multiple redox cycles of **PDI-1** were performed by repeated additions of 1 μL of a $Na_2S_2O_4$ solution (400 mM in borate buffer) under stirring at time intervals of 20 min., in the "slow cycling", (i.e., allowing time for hierarchical growth, leading to colloidally stable solutions of 10 μM) or 3 min., in the "fast cycling", (i.e., leading to complete precipitation). The redox cycles do not change the pH measurably (verified up to 7 cycles).

Seeding experiments. An aliquot (0.5 mL) of 100 μM **PDI-1** (aged for 10 min. after one redox cycle) was added to 2 mL of just oxidized 100 μM **PDI-1** solution (prepared as described above).

Confocal measurements. Confocal micrographs were taken by using Zeiss LSM 710 confocal microscope system with 63x magnification, numerical aperture, NA, 1.3 of Zeiss LCI Plan-NEOFLUAR immersion objective lens (Zeiss GmbH). The samples were excited by continuous-wave laser at 488 nm. The emission was measured from 500 nm to 700 nm using a spectral detector. Measurements were performed on as-prepared a 100 μM **PDI-1** and at different time intervals after oxidation (1 redox cycle).

UV-Vis measurements. UV-Vis spectra were taken by using a JASCO V-670 spectrometer equipped with a Peltier system as a temperature controller. When not otherwise specified, spectra were recorded in a 0.2 cm quartz cuvette at 25 ºC.

Fluorescence measurements. Emission spectra were recorded with a Fluorolog®-3 spectrofluorometer by exciting at 488 nm and recording between 500 nm and 750 nm.

Dynamic light scattering (DLS). The intensity autocorrelation functions $g^{(2)}(q,\tau) \equiv \langle I(q,0)I(q,\tau)\rangle / \langle I(q,0)^2\rangle$ were measured on a home-built light scattering setup with an ALV7002 digital correlator using a laser diode at λ = 639 nm at a wavevector $q = 0.0185\ nm^{-1}$ (90° scattering angle). Measurements were performed on as-prepared 100 μM **PDI-1**, its reduced form **PDI-1**$^{2-}$, and every 30 s or 60 s for 20 min. immediately after oxidation (for each redox cycle). The relaxation dynamics were analysed by the inverse Laplace transformation $g^{(1)}(\tau) = \int_0^\infty H(\Gamma)e^{-\Gamma t}d\Gamma$ where

$g^{(1)} = \sqrt{g^{(2)} - 1}$. Hydrodynamic radii R_H were then calculated using the Stokes-Einstein relation $R_H = k_B T/(6\pi\eta D)$ where $D = 1/(\tau q^2)$.

Atomic force microscopy (AFM). Measurements were performed under ambient condition using a Bruker Veeco Dimension 3100 AFM microscope with Nanoscope IV controller, operating in tapping mode. Silica probes Bruker TESPAW-V2 with a resonance frequency of ~360 kHz and a spring constant of ~80 Nm^{-1} were used. The samples were prepared by spin-coating (3000 rpm, 1 min.) on freshly cleaved Mica surfaces 100 µM **PDI-1** solutions soon after oxidation (1 redox cycle) and after further 20 min. ageing. The height of the **PDI-1** assemblies in the different samples was determined by cross section analysis of at least 50 fibers.

Section 3. Electrochemical analysis.

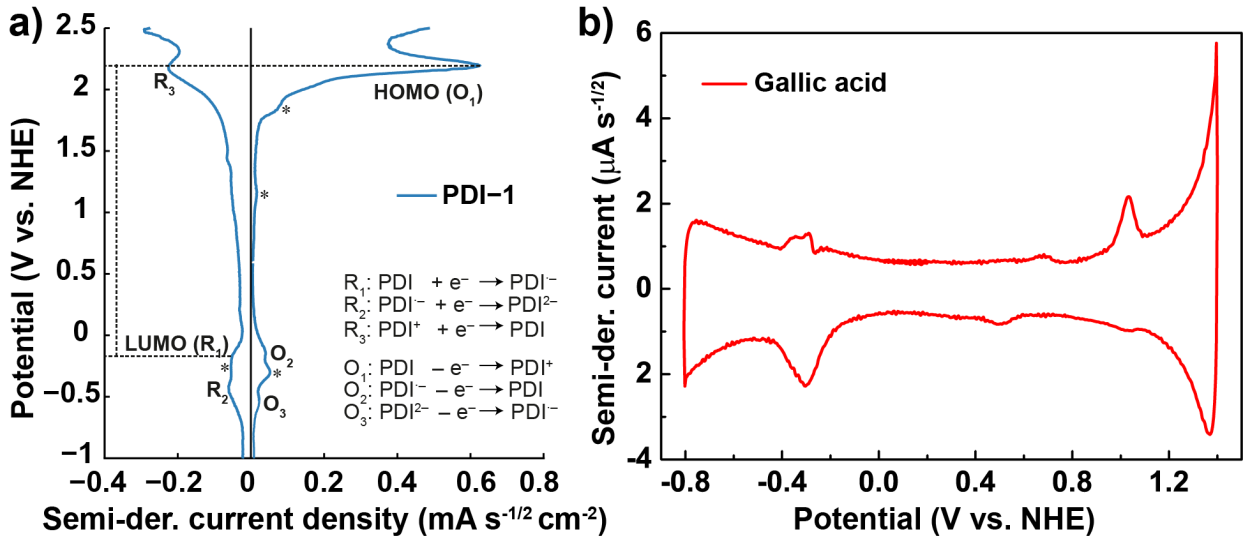

Fig. S1. (a) Semi-derivative cyclic voltammogram of 200 µM **PDI-1** in 0.1 M $TBAPF_6$ in DCM at 100 mV/s. The HOMO and LUMO levels are marked by the first oxidation and reduction peaks respectively. The redox peaks due to the gallic moiety are marked by * (b) Semi-derivative cyclic voltammogram of 2 mM gallic acid in 0.1 M KCl in water at 100 mV/s

The HOMO-LUMO levels of **PDI-1** can be related to the standard potentials of reduction and oxidation of the molecule.[1] From the semiderivative of a cyclic voltammogram at 100 mV/s, and a concentration of 200 µM (Fig. S1a), we observed two reduction peaks from the PDI core at -0.20 V (the LUMO) and -0.42 V, and their corresponding re-oxidation peaks at -0.54 V for the return of the dianion to the radical, and -0.14 V for the radical returning to the neutral molecule. This difference in the forward and reverse sweeps decreased with lower scan rates as expected for a quasi-reversible system. There is a coupled, reversible redox peak at -0.25 V with the return (positive) peak at -0.3 V which is due to the reduction of the gallic moiety of **PDI-1**, as can be seen in Fig. S1b for the semiderivative of a cyclic voltammogram of 2 mM gallic acid in water. At positive potentials, the molecule undergoes quasi-reversible oxidation at 2.20 V (HOMO), and we observe two further irreversible oxidation peaks of two of the hydroxyl groups from the gallic ligands[2] at 1.16 V, and 1.84 V. We can only detect the first gallic acid oxidation peak in water at 1.03 V, as at higher potentials the peaks are masked by the decomposition of water. The HOMO-LUMO redox gap for **PDI-1** is 2.40 V, or equivalently 517 nm, in agreement with the UV-Vis absorption spectra.

Section 4. Spectroscopic measurements

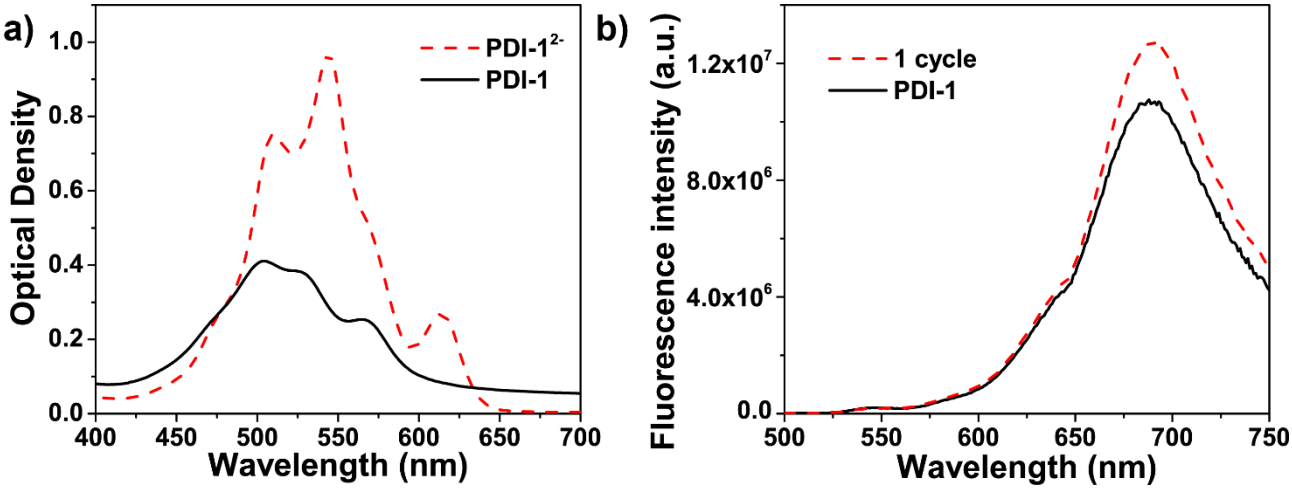

Fig. S2. (a) UV-Vis spectra of 100 μM **PDI-1** (black solid line) and **PDI-1**$^{2-}$ (red dashed line) solutions in 50 mM borate buffer pH 8 (optical path 0.2 cm). (b) Fluorescence emission spectra of 100 μM **PDI-1** as-prepared (black solid line) and aged 20 min. after 1 redox cycle (red dashed line).

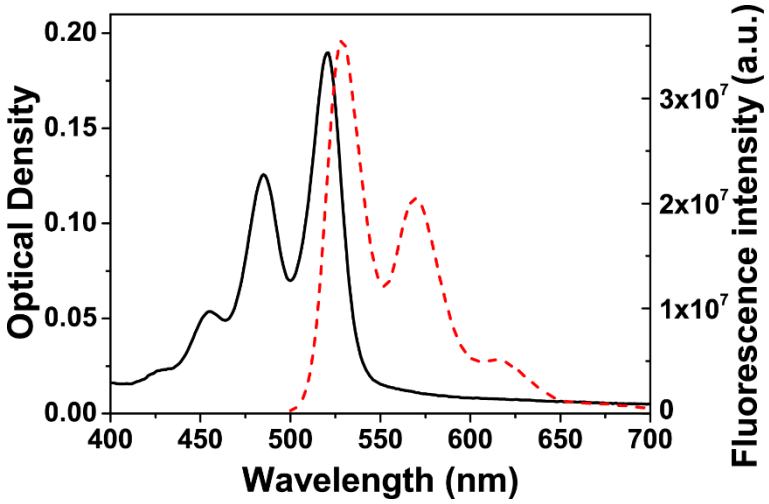

Fig. S3. UV-Vis (black line) and fluorescence (red dash line) spectra of 5 μM **PDI-1** in acetonitrile (optical path 1 cm), showing the typical vibronic pattern of the S0→S1 transition for monomeric PDIs (between 400 nm and 600 nm), and the mirror image emission (between 500 nm and 650 nm).

Section 5. Study of the assembly of PDI-1^{2-}

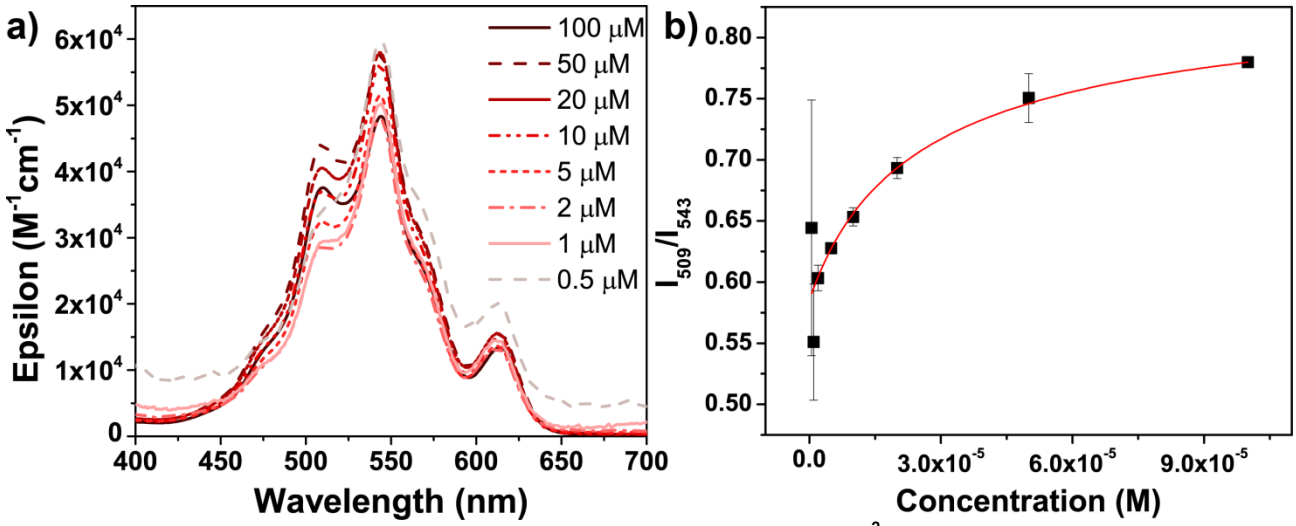

Fig. S4 (a) UV-Vis spectra recorded at 25 °C for different concentrations of **PDI-1**$^{2-}$ (from 0.5 μM to 100 μM, optical path 0.2 – 1 cm) in 50 mM borate buffer (spectra normalized to show the molar extinction coefficient). (b) Ratio of peak intensities at 509 nm and 543 nm (I_{509nm}/I_{543nm}), relative to the absorption spectra of in panel (a), as a function of **PDI-1**$^{2-}$ concentration (black squares). Error bars show standard deviations. The red solid line corresponds to the fitting with a concentration-dependent isodesmic (Equal K model),[3] from which a $K_{eq.}$ = 2.0 x 10^4 ± 3 x10^3 M^{-1} was obtained.

The UV-Vis spectra of **PDI-1**$^{2-}$ were recorded under N_2 atmosphere at different concentrations (from 0.5 μM to 100 μM, while ensuring **PDI-1**$^{2-}$ was staying reduced at all times) at 25 °C. The ratio of the peak intensities I_{509nm}/I_{543nm} was calculated for all the spectra and plotted against the concentration of **PDI-1**$^{2-}$ (see Fig S4b). The data in Fig. S4b were fitted using a concentration-dependent isodesmic model,[3] using the following expression,

$$R(C) = \left[1 - \left(\frac{2K_{eq}C + 1 - \sqrt{4K_{eq}C + 1}}{2K_{eq}^2C^2}\right)\right] \times \left(R_{pol} - R_{mon}\right) + R_{mon}$$

where $R(C)$ = I_{509nm}/I_{543nm} at a given concentration; $K_{eq.}$ is the equilibrium constant for the self-assembly, C is the total concentration of **PDI-1**$^{2-}$, R_{pol} corresponds to the ratio $(I_{509nm}/I_{543nm})_{pol}$ for the fully polymerized **PDI-1**$^{2-}$, and R_{mon} corresponds to the intensity ratio $(I_{509nm}/I_{543nm})_{mon}$ for monomeric **PDI-1**$^{2-}$. The fit gave a K_{eq} = 2.0 x 10^4 ± 3 x10^3 M^{-1}, with an adjusted R^2 > 0.999. Further studies are needed to eliminate other possible self-assembly mechanisms (i.e., anti-cooperative or cooperative).

Section 6. AFM images

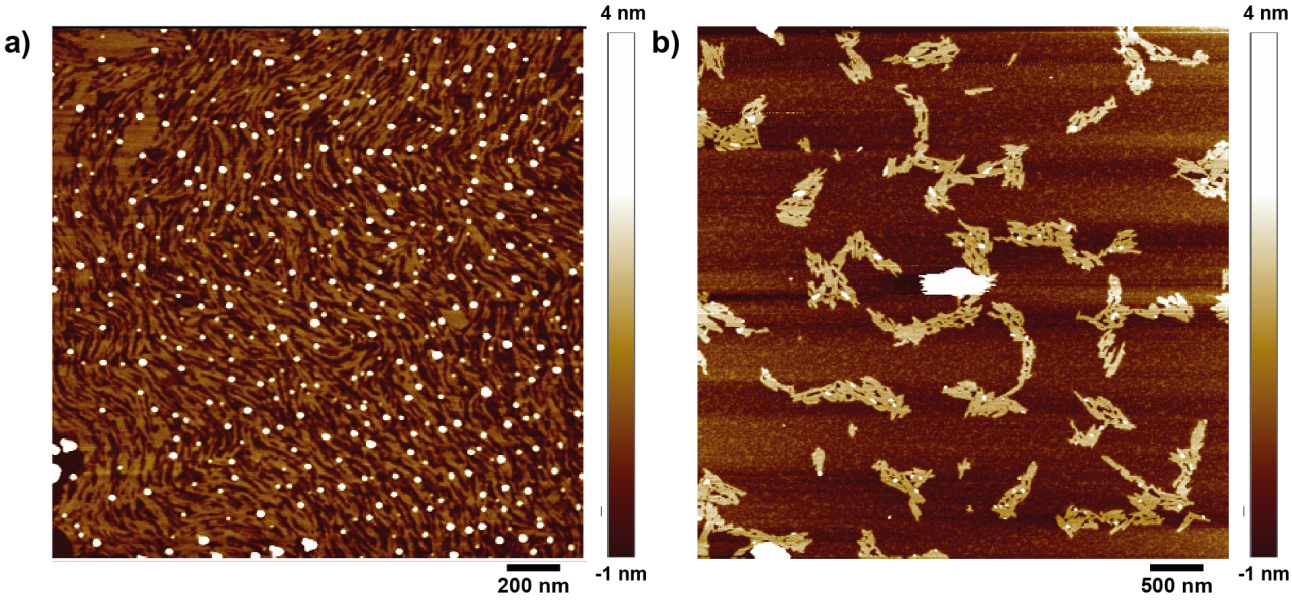

Fig. S5. AFM images of a 100 µM **PDI-1** solution in 50 mM borate buffer spin-coated on mica (a) immediately after 1 redox cycle. (b) after 20 min. ageing following 1 redox cycle.

Section 7. Autocatalytic growth of PDI-1 assemblies

To shed more light on the autocatalytic nucleation of **PDI-1** we fit the time evolution of the normalized optical density (OD) to a minimal 2-step autocatalytic model first proposed by Watzky and Finke,[4] which has been used to analyze the self-assembly kinetics of different proteins,[5]

$$A \overset{k_1}{\rightarrow} B$$
$$A + B \overset{k_2}{\rightarrow} 2B$$

where *A* is the concentration of a (precatalytic) species that is smaller than the critical size for nucleation, and *B* is the concentration of the catalytic species that grows exponentially. The model describes two pseudoelementary steps, namely: i) nucleation with rate k_1, and ii) growth/elongation with rate k_2. Both of which are irreversible, which for our system is justified since no monomer is present after completion of the assembly process.

The kinetics of assembly of **PDI-1** just after 1 redox cycle was measured at different concentrations (i.e., 50 µM, 20 µM, and 10 µM) as can be seen in Fig. S6. We assume that species *B* is dominant in the signal of OD (where OD is normalized between 0 and 1), and using the analytical expression for the 2-step model[5] we obtained the following expression that was used to fit the results in Fig. S6:

$$B = \left(A_0 - \frac{\frac{k_1}{k_2} + A_0}{1 + \frac{k_1}{k_2 A_0} e^{(k_1 + k_2 A_0)t}} \right) / A_0$$

The experiments at 50 µM and 20 µM could be fitted with the same values for k_1 and k_2 (0.02442 ± 0.003 min^{-1} and 0.02112 ± 0.0008 μM^{-1} min^{-1}, respectively). The lower concentration experiments at 10 µM resulted in a significantly slower (~19 times) nucleation event with a k_1 of 0.00128 ± 0.0002 min^{-1}. The adjusted R^2 was > 0.99 for all fits. Based on this analysis (and on the seeding experiments

described in the main text) we conclude that the assembly of **PDI-1** is indeed autocatalytic, but further kinetic studies are needed to elucidate the exact growth mechanism.

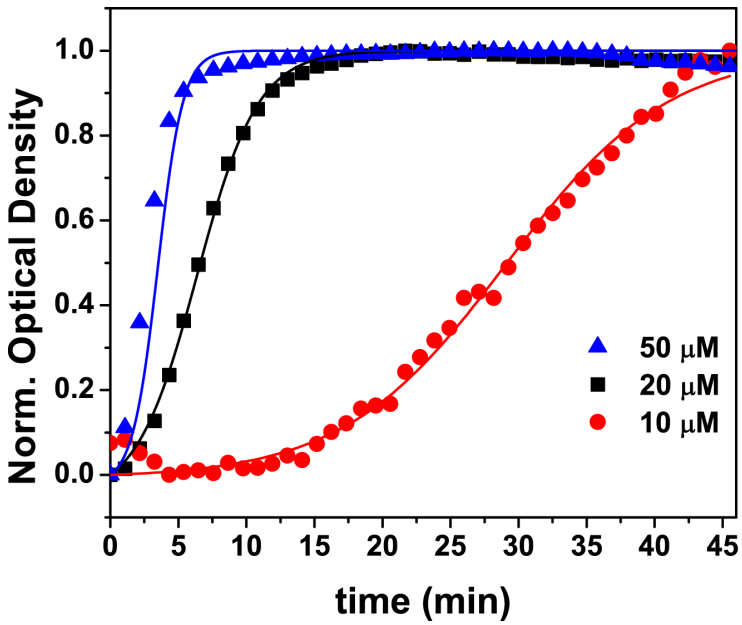

Fig. S6. Time evolution of the normalized optical density (OD) at 528 nm immediately after 1 redox cycle for **PDI-1** solutions at different concentrations (symbols). The solid lines correspond to the fitting of the experimental data using the minimal 2-step model described in section 7 (above).

Section 8. Cycling experiments at lower concentration

Cycling experiments at a lower **PDI-1** concentration (i.e., at 10 μM) also resulted in colloidally stable solutions (compare panel a and b, Fig. S7). The OD intensity of this stable solution is equal at the peak maximum (508 nm, Fig. S7c) as compared to the one prepared from a 100 μM initial concentration (Fig. S7a). However, the vibronic structure is rather different, and the R_H is smaller as well (cf. red solid vs black dashed line, Fig. S7c,d), suggesting a difference in molecular packing. As explained earlier, at 10 μM (vs. 100 μM) the **PDI-1**$^{2-}$ species are much less assembled (cf. Fig. S4b). Therefore, the nucleation (and subsequent autocatalytic growth) is different, apparently leading to differently assembled structures. Taken together, of importance to pathway selection of our system are time, concentration, and number of cycles, which all affect the hierarchical growth and final outcome of the **PDI-1** assemblies.

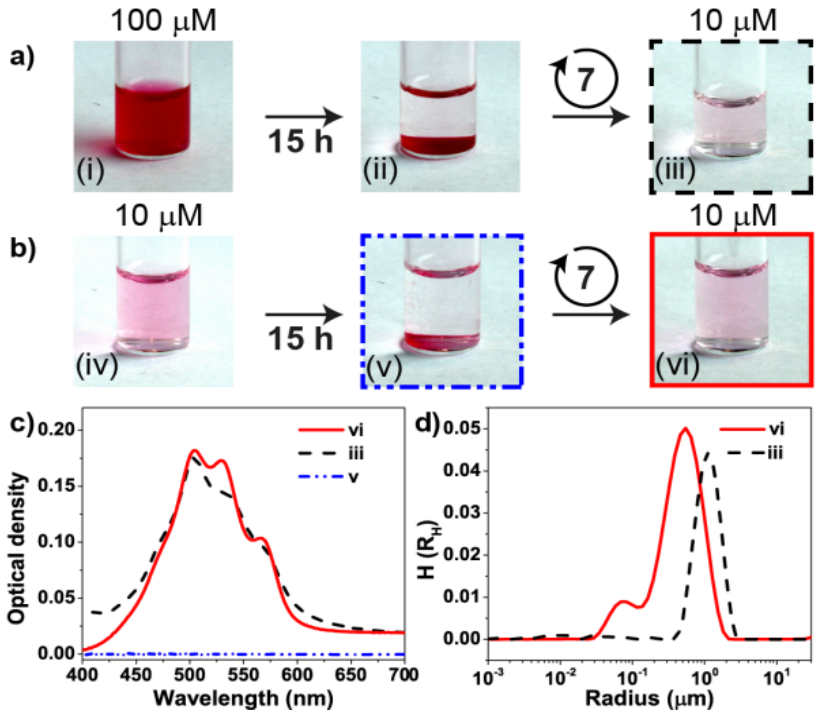

Fig. S7. (a,b) Pathway selection in **PDI-1** self-assembly starting at 100 μM and 10 μM, respectively: (i, iv) as-prepared solutions; (ii, v) overnight precipitation; (iii, vi) colloidally stable assemblies after redox cycling (7 times at 20 min intervals) (c,d) UV-Vis spectra and hydrodynamic radii obtained for soluble assemblies corresponding to iii (red solid line) and vi (dashed black line). The dash-dot blue line in (c) is the UV-Vis spectrum of v, confirming complete precipitation overnight.

References

1 F. Würthner, C. R. Saha-Möller, B. Fimmel, S. Ogi, P. Leowanawat and D. Schmidt, *Chem. Rev.*, 2015. **DOI:** 10.1021/acs.chemrev.5b00188

2 M. K. Carter, *J. Mol. Struct.*, 2007, **831**, 26–36.

3 R. B. Martin, *Chem. Rev.*, 1996, **96**, 3043–3064.

4 M. A. Watzky and R. G. Finke, *J. Am. Chem. Soc.*, 1997, **119**, 10382–10400.

5 A. M. Morris, M. A. Watzky and R. G. Finke, *Biochim. Biophys. Acta BBA - Proteins Proteomics*, 2009, **1794**, 375–397.